Contents lists available at ScienceDirect

Transactions of Nonferrous Metals Society of China

36(2026) 287−297

www.tnmsc.cn

Effect of hydrogen sulfide on reductive leaching of chalcopyrite by copper

Xin SUN [a,b], Rui LIAO [a,b,**], Zu-chao PAN [a], Yi-sheng ZHANG [a,b], Mao-xin HONG [a,b], Yan-sheng ZHANG [a,b], Jun WANG [a,b,*], Guan-zhou QIU [a,b]

[a] School of Minerals Processing & Bioengineering, Central South University, Changsha 410083, China;
[b] Key Laboratory of Biohydrometallurgy, Ministry of Education, Central South University, Changsha 410083, China

Abstract: A series of leaching and electrochemical experiments were conducted to elucidate the critical role of hydrogen sulfide (H_2S) in copper-driven reduction of chalcopyrite. Results demonstrate that in the absence of H_2S, metallic copper converts chalcopyrite into bornite (Cu_5FeS_4). However, the introduction of H_2S promotes the formation of chalcocite (Cu_2S) by altering the oxidation pathway of copper. Electrochemical analysis demonstrates that the presence of H_2S significantly reduces the corrosion potential of copper from 0.251 to −0.223 V (vs SHE), reaching the threshold necessary for the formation of Cu_2S. Nevertheless, excessive H_2S triggers sulfate reduction via the reaction of $8Cu+H_2SO_4+3H_2S=4Cu_2S+4H_2O$ (ΔG=−519.429 kJ/mol at 50 °C), leading to inefficient copper utilization.
Keywords: chalcopyrite reduction; copper; hydrogen sulfide; chalcocite

1 Introduction

As primary copper sulfide mineral, chalcopyrite ($CuFeS_2$) constitutes approximately 70% of global copper reserves [1]. The hydrometallurgical processing of $CuFeS_2$ has attracted significant attention due to its economic and environmental advantages [2,3].

Conventional hydrometallurgical approaches include oxidative and reductive methods. During oxidative leaching, however, $CuFeS_2$ rapidly forms a passivation layer that impedes charge transfer and limits leaching efficiency [4−9]. Although effective under specific conditions (e.g., high acidity or microbial intervention), oxidative leaching often requires extended durations and may be unfeasible economically [10−14].

In contrast, the reductive leaching converts $CuFeS_2$ into more leachable phases (e.g., chalcocite, Cu_2S) [15], achieving >95% extraction within hours under controlled pH and redox potential (ORP) [16,17]. This two-step process (reduction followed by oxidation) was first proposed in the 1970s [18]. The reduction step involves the following electrochemical reactions [19]:

$$5CuFeS_2+12H^++4e=Cu_5FeS_4+4Fe^{2+}+6H_2S \quad (1)$$

$$2CuFeS_2+6H^++2e=Cu_2S+2Fe^{2+}+3H_2S \quad (2)$$

$$CuFeS_2+4H^++2e=Cu+Fe^{2+}+2H_2S \quad (3)$$

In general, reductants such as aluminum [20], iron [15], vanadium(II) [21], and chromium(II) [22] have been explored, and their industrial adoption remains limited by low utilization efficiency (30%−40% for Fe in acidic media [23,24]) and the need for essential purification of introduced metal ion impurities. Particularly, copper (Cu) presents distinctive advantages due to its controlled acid reactivity, which effectively suppresses the side

Corresponding author: *Jun WANG, Tel: +86-731-88876557, E-mail: wjwq2000@126.com;
**Rui LIAO, Tel: +86-731-88836041, E-mail: csuliaorui@163.com
https://doi.org/10.1016/S1003-6326(25)66964-0
Received 28 May 2024; accepted 25 March 2025

reactions while facilitating closed-loop recovery of spent Cu through oxidative leaching−electrodeposition cycles. Despite these merits, previous studies have identified challenges in galvanic coupling between Cu and $CuFeS_2$, particularly under agitation or high pulp density [18]. Notably, H_2S and ferrous ions may form passivating FeS layers, further inhibiting reactions [25,26]. Additionally, MARTINEZ-GOMEZ et al [27] suggest that a significant amount of hydrogen sulfide (H_2S) reacts with dissolved oxygen to produce elemental sulfur, which then attaches to the surface of the particles and inhibits further transformation. It is reported the sulfide ions reduce the electrode potential of Cu to elevate its electron-donating capacity [28]. However, the mechanistic role of H_2S in Cu-driven $CuFeS_2$ reduction remains poorly understood. Therefore, understanding the role of H_2S can provide a theoretical basis for determining its optimal concentration range, thereby potentially increasing the pulp density that the process can handle and enhancing the overall treatment capacity.

To address this knowledge gap, we investigated the critical role of H_2S in $CuFeS_2$ reduction process. Specifically, the effects of stirring speed, atmosphere, and initial H_2S concentration were systematically examined during the reduction of $CuFeS_2$ by Cu in sulfuric acid solution, aiming to identify the primary factors governing Cu utilization efficiency and $CuFeS_2$ conversion rates. Galvanic coupling and electrochemical tests were conducted on Cu and $CuFeS_2$ electrodes both in the absence and presence of H_2S, to elucidate the interaction mechanisms among H_2S, Cu, and $CuFeS_2$, as well as the reductive phase transition of $CuFeS_2$. Based on these findings, a reaction model integrating H_2S, Cu, and $CuFeS_2$ was proposed, supported by thermodynamic analysis. The results reveal a novel mechanism by which H_2S modulates the Cu oxidation pathway and enhances the electron-donating capacity of Cu during $CuFeS_2$ reduction.

2 Experimental

2.1 Materials

The $CuFeS_2$ sample was sourced from Hunan Province, China. X-ray diffraction (XRD) analysis (Fig. 1) confirmed its high purity, with only trace amounts of quartz and pyrite detected. The chemical composition, as given in Table 1, revealed 31.49% Cu, 29.23% Fe, and 35.06% S. For the galvanic tests, $CuFeS_2$ and Cu electrodes (26 mm in diameter) were polished and encapsulated in silicone, leaving only the reaction surface exposed. In the leaching experiments, $CuFeS_2$ particles (38−74 μm) and Cu powder (5−10 μm) were used. All other reagents were of analytical grade (99.7% in purity). Deionized water with a resistivity of 18.25 MΩ·cm was used for all dissolution processes.

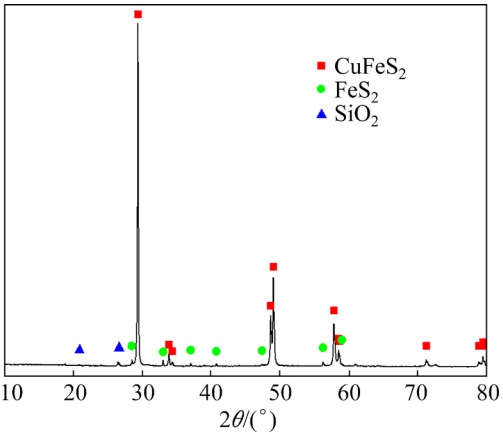

Fig. 1 XRD pattern of $CuFeS_2$ sample

Table 1 Chemical composition of $CuFeS_2$ sample (wt.%)

S	Cu	Fe	Si	Ca	Al	Mg	Others
35.06	31.49	29.23	1.37	0.40	0.17	0.18	2.10

2.2 Methods

2.2.1 Reductive leaching

The reductive leaching experiments were conducted in a 500 mL three-neck flask maintained at (50±1) °C using a thermostatic water bath with magnetic stirring. A 200 mL gas-tight syringe was installed on the central neck to allow pressure equilibration and gas sampling. The standard reaction system contained 200 mL H_2SO_4 solution (15 g/L, three-times stoichiometric excess), 2.00 g $CuFeS_2$ sample, and 0.69 g Cu powder (m(Cu):m($CuFeS_2$ sample)=0.345:1, based on stoichiometry in Eq. (2)). This setup ensured copper availability while facilitating precise tracking of the Cu consumption efficiency.

Solution redox potential (ORP) was monitored in real-time using a Pt electrode calibrated against the standard hydrogen electrode (SHE). Periodic

50 μL aliquots were collected for ICP-AES analysis (Agilent 720ES) to determine Cu and Fe concentrations, with sample volume loss compensated by replenishing an equivalent amount of H_2SO_4. After leaching, H_2 concentrations in 100 mL headspace samples were measured using gas chromatography (Agilent 7890B), whereas filtered solutions were analyzed for sulfate content via ion chromatography (Thermo ICS 2100). Each experiment was independently repeated twice, and the data from these replicates were averaged and presented with standard deviations to demonstrate consistency across measurements.

2.2.2 Electrochemistry and galvanic couple

Open-circuit potential (OCP) measurements were conducted using an Ag/AgCl (saturated KCl) reference electrode, and the recorded values were converted to the SHE scale. Galvanic coupling currents between Cu and $CuFeS_2$ electrodes were measured using a CHI760E electrochemical workstation (Shanghai Chenhua) in zero-resistance ammeter (ZRA) mode. The three-electrode system used 300 mL of 15 g/L H_2SO_4 electrolyte maintained at 50 °C. Before the measurements, dissolved oxygen was removed by purging the electrolyte with nitrogen (N_2) for 20 min.

2.2.3 Characterization methods

The X-ray diffraction (XRD) patterns of each powder sample were obtained using an X-ray diffractometer (Advance D8/Bruker) equipped with a Cu K_α radiation source (40 kV, 40 mA). The samples were scanned from 10° to 90° at a step size of 0.02° and a scan speed of 1 s per step. Phase identification was performed using MDI Jade 9.0 by matching the experimental XRD patterns with those retrieved from the standard powder diffraction database published by the International Centre for Diffraction Data (ICDD PDF).

Raman spectroscopy analysis was performed using Raman microscope (Renishaw InVia Qontor) with an excitation wavelength of 532 nm [29]. The samples were examined using a scanning electron microscope (SEM, TESCAN/TIMA GMH FEG) and an energy-dispersive X-ray spectrometer (EDS) to observe their morphological changes and microarea elemental composition. The FactSage EpH Module was used to calculate pourbaix diagrams for the heterophase system of $CuFeS_2$−Cu−H_2SO_4−H_2O [30].

3 Results and discussion

3.1 Factors influencing reductive leaching

The effects of varying stirring intensities, atmospheres, and the presence of H_2S were systematically investigated. The reduction of $CuFeS_2$ in a sulfuric acid system, as demonstrated by Eq. (2), leads to the formation of H_2S and ferrous ion. The extent of $CuFeS_2$ conversion can be quantitatively assessed through the measurement of ferrous ion concentration variations in the aqueous solution.

3.1.1 Agitation

In non-stirred systems (Fig. 2(a)), $CuFeS_2$ reduction was facilitated, resulting in the formation of a porous Fe-depleted/Cu-enriched layer with a thickness of 3.8 μm (Fig. 3). Conversely, under stirring at 150 r/min (Fig. 2(b)), Cu was completely dissolved without $CuFeS_2$ reduction, which was attributed to oxygen ingress [31]. The conversion rate of $CuFeS_2$ and the utilization rate of Cu were significantly influenced by the stirring and atmospheric conditions.

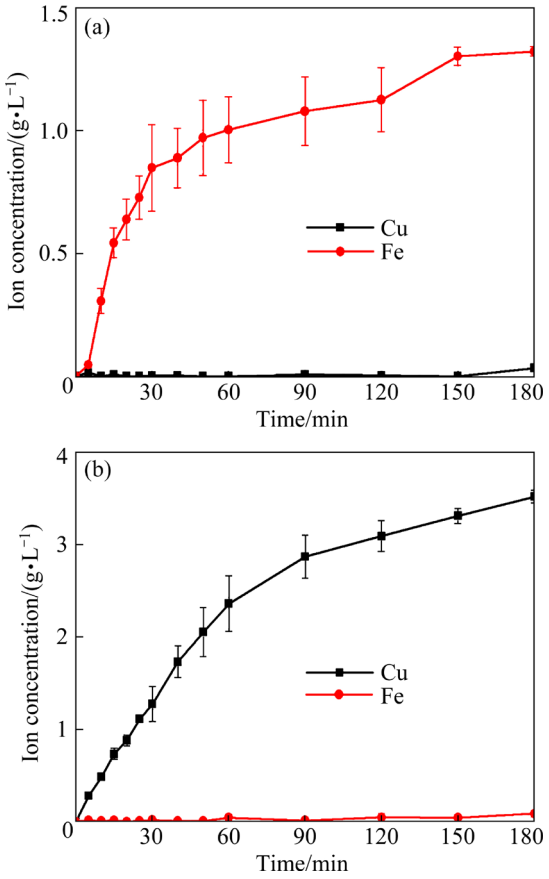

Fig. 2 $CuFeS_2$ conversion under (a) non-stirred and (b) stirred (150 r/min) conditions

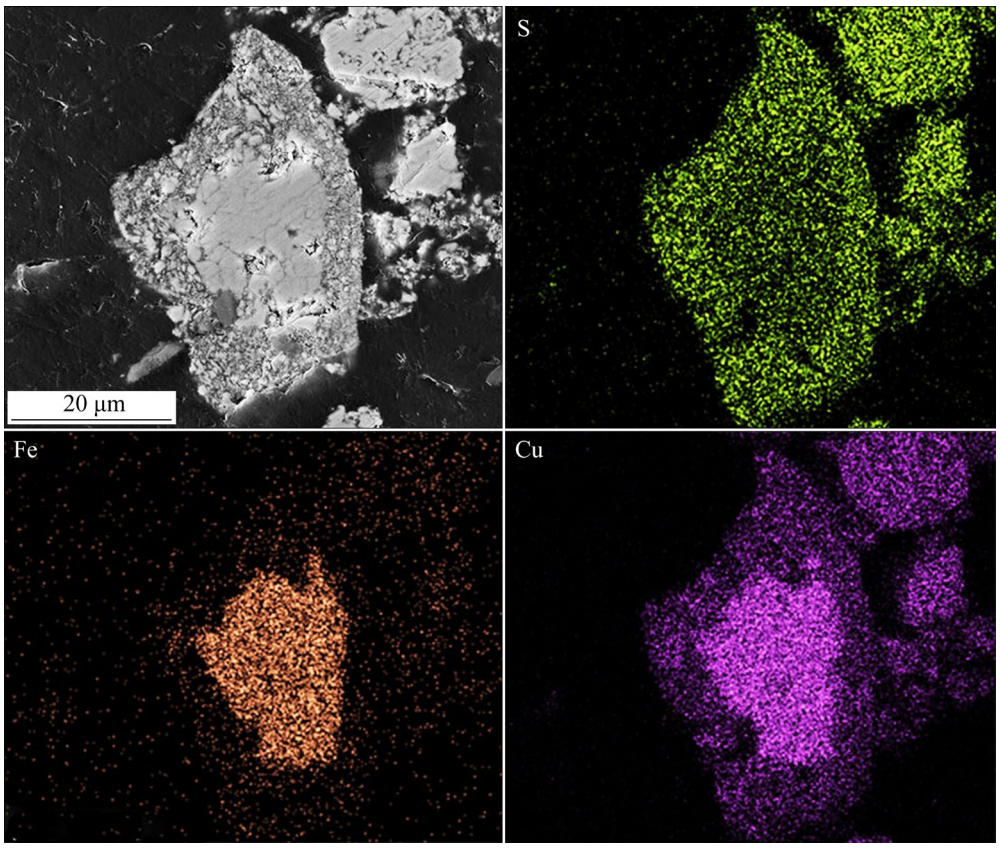

Fig. 3 Cross-sectional SEM−EDS mapping of leached $CuFeS_2$ (non-stirred)

The influence of agitation rate on $CuFeS_2$ reduction was systematically investigated in an oxygen-excluded closed system (Fig. 4). The leaching process universally displayed three characteristic stages: (1) initial slow reaction, (2) rapid acceleration, and (3) progressive deceleration. The exponential acceleration phenomenon can be attributed to two potential mechanisms: (1) The hydration layer displacement process involves the initial shielding of particle surfaces by bound water molecules, followed by the progressive removal of this hydrated layer, which subsequently exposes fresh reactive sites on the surface; (2) Pitting-driven surface roughening occurs when localized corrosion creates micro-pits, which geometrically amplify the effective reaction surface area.

A systematic investigation revealed a positive correlation between agitation intensity and the duration of the reaction induction. Under 30 r/min conditions, the induction phase lasted 5 min approximately, progressively extending to 10 and 15 min as rotational speeds increased to 50 and 100 r/min, respectively. Significantly, sustained low-reactivity behavior was observed at 150 r/min

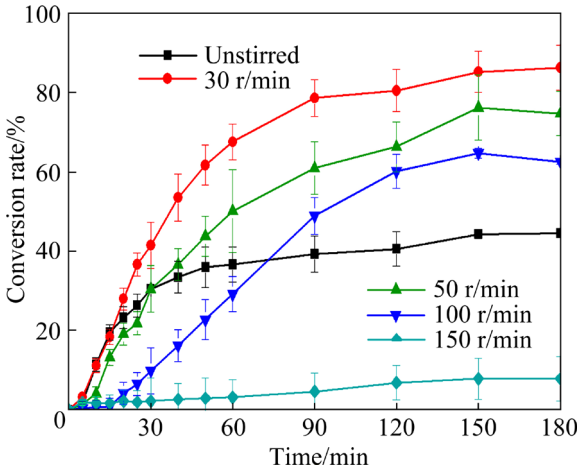

Fig. 4 Time-dependent $CuFeS_2$ conversion rates under different agitation speeds in closed system

agitation. This phenomenon is presumably attributed to vigorous stirring enhancing particle hydration while simultaneously hindering direct contact between $CuFeS_2$ and Cu. In the absence of stirring, the reduction reaction of $CuFeS_2$ showed a declining trend after 30 min, which is likely caused by localized H_2S accumulation. Such excessive H_2S accumulation may lead to reaction passivation.

3.1.2 Atmosphere

A series of experiments were conducted at the optimal rotation speed of 30 r/min to investigate the influence of atmosphere on $CuFeS_2$ reduction, using continuous injection of air or N_2 at a flow rate of 0.4 L/min. As shown in Fig. 5(a), the $CuFeS_2$ conversion rate exceeded 97% under N_2 purging (0.4 L/min), alongside a significant drop in ORP to −295 mV (Fig. 5(b)). Phase analysis of leaching residue (Fig. 5(d)) confirmed complete conversion of $CuFeS_2$ to Cu_2S, with no detectable residual $CuFeS_2$. These results indicate that N_2 atmosphere effectively facilitates near-complete conversion of $CuFeS_2$ to Cu_2S by maintaining reducing conditions.

Under continuous aeration, the ORP increased to 265 mV within 40 min (Fig. 5(c)), which facilitated oxygen-mediated oxidation of metallic Cu and led to terminating of the target reaction, despite achieving a $CuFeS_2$ conversion of 74.61%. XRD analysis (Fig. 5(d)) showed no evidence of elemental sulfur or polysulfide species in the residue under air-purging conditions. Instead, roxbyite was identified as the dominant phase, indicating progressive oxidation of Cu_2S.

The oxidation of Cu_2S proceeds through a stepwise pathway involving nonstoichiometric sulfides as intermediates. With increasing oxidation, the following sequential phase transitions: djurleite ($Cu_{1.93-1.96}S$), roxbyite ($Cu_{1.72-1.82}S$), digenite ($Cu_{1.75-1.78}S$), anilite ($Cu_{1.75}S$), geerite ($Cu_{1.5-1.6}S$), spionkopite ($Cu_{1.4}S$), and yarrowite ($Cu_{1.1}S$) [32]. The initial oxidation threshold for the conversion of Cu_2S to nonstoichiometric sulfide is above 345 mV [33]. In this study, the final ORP under air atmosphere reached 401 mV (Fig. 5(b)), which exceeded this threshold and drove the formation of $Cu_{1.82}S$ as the terminal product.

3.1.3 H_2S concentration

Based on previous studies, sodium sulfide (Na_2S) was introduced into sulfuric acid to produce H_2S in situ. The reductive transformation of $CuFeS_2$ mediated by Cu was systematically investigated across a range of initial Na_2S concentrations (Fig. 6).

Significantly, under the stirred conditions (30 r/min), the addition of Na2S eliminated the initial reaction lag phase, demonstrating the role of

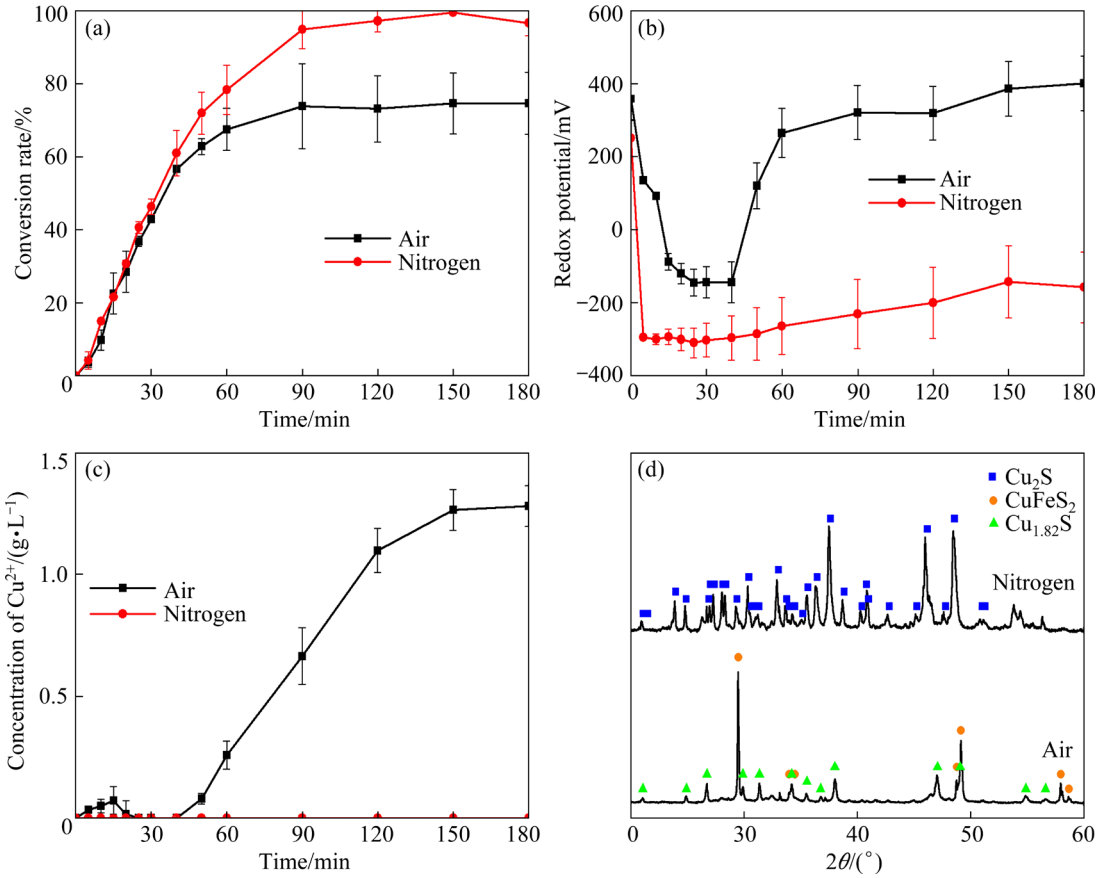

Fig. 5 Effects of atmospheric conditions: (a) $CuFeS_2$ conversion rate; (b) ORP evolution; (c) Dissolved Cu concentration; (d) XRD patterns of leaching residue

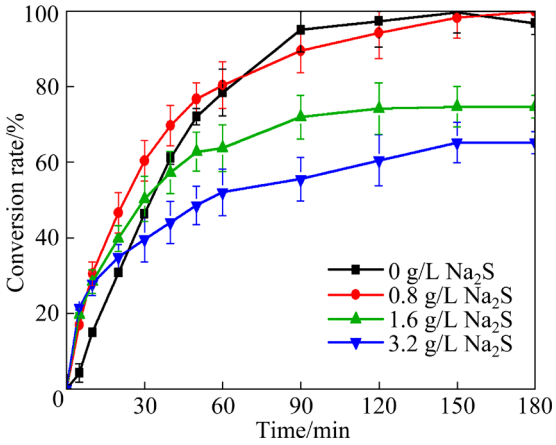

Fig. 6 $CuFeS_2$ conversion rates under varying initial Na_2S concentrations

H_2S in accelerating the reaction kinetics. In the electrically assisted reduction process, although $CuFeS_2$ acts as the primary reaction site, H_2S does not exhibit any catalytic effect on this mineral phase. These findings suggest that H_2S primarily interacts with the cathodic Cu surface rather than directly engaging in $CuFeS_2$ reduction.

When the Na_2S concentration was set as 1.6 and 3.6 g/L, the $CuFeS_2$ conversion rates dropped to 74.6% and 65.1%, respectively, after 3 h of reaction. According to XRD analysis (Fig. 7), no metallic Cu was detected in the residues from the 1.6 g/L Na_2S system, suggesting that excessive Cu consumption occurred under high H_2S concentrations.

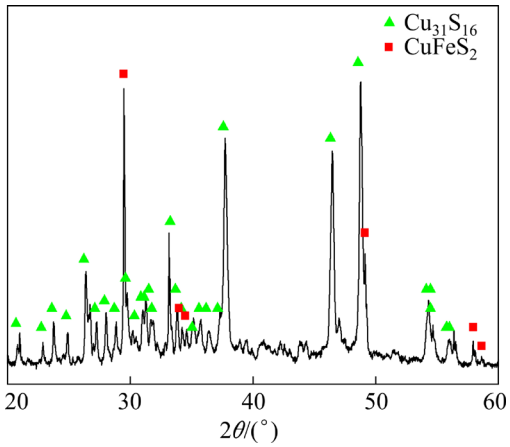

Fig. 7 XRD pattern of leaching residue obtained at initial Na_2S concentration of 1.6 g/L

To elucidate the underlying mechanism, the hydrogen (H_2) content in headspace gas and sulfate ion concentration in the solution were analyzed after the reaction (Fig. 8). In the absence of Na_2S, H_2 comprised only 5.03% of the headspace gas (approximately 300 mL), with 2% of the Cu consumed in H_2 generation. Through galvanic coupling, Cu was primarily driven to reduce $CuFeS_2$, while residual free Cu reacted with H_2S produced from $CuFeS_2$ reduction, resulting in trace H_2 formation. However, increasing Na_2S concentrations progressively inhibited hydrogen production and enhanced sulfate consumption. Previous studies have shown that H_2S reacts with sulfuric acid to form elemental sulfur or SO_2 [34], leading to acid depletion. Notably, the absence of elemental sulfur in XRD patterns (Fig. 7) indicates that sulfate reduction likely occurred through Cu−H_2S interactions. This parasitic reaction not only consumed Cu but also depleted acid resources, thereby accounting for the reduced hydrogen yield.

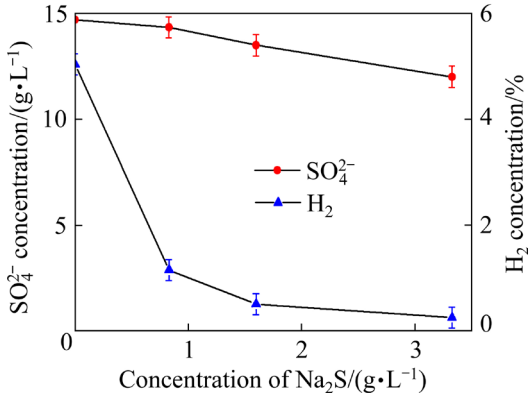

Fig. 8 Hydrogen concentration in reactor headspace and sulfate ion concentration in solution at reaction completion

3.2 Promoting effect of hydrogen sulfide by galvanic tests

In the electrochemical systems, electrons spontaneously transfer from materials with lower corrosion potentials to those with higher potentials. Open-circuit potential (OCP) measurements provide direct quantification of this electron transfer behavior. To investigate the effects of H_2S, Na_2S (20 mg) was incrementally added at 1 min intervals over three sequential doses. Following Na_2S addition, the OCP of $CuFeS_2$ dropped from 0.456 to 0.284 V (Fig. 9(a)), whereas metallic Cu exhibited a shifted OCP from 0.251 to −0.223 V (vs SHE), thereby amplifying the potential difference between the two materials from 0.2 to 0.5 V. Comparative analysis of galvanic currents (Fig. 9(b)) highlighted significant differences between

Na_2S-free and Na_2S-supplemented systems. Under unmodified reaction pathways, current−voltage relationships generally follow linear proportionality. Notably, Na_2S addition boosted the electromotive force by 2.5 times and elevated current density by an order of magnitude. These results demonstrate that H_2S fundamentally modifies the reaction pathway, likely through modulating of interfacial electron transfer kinetics.

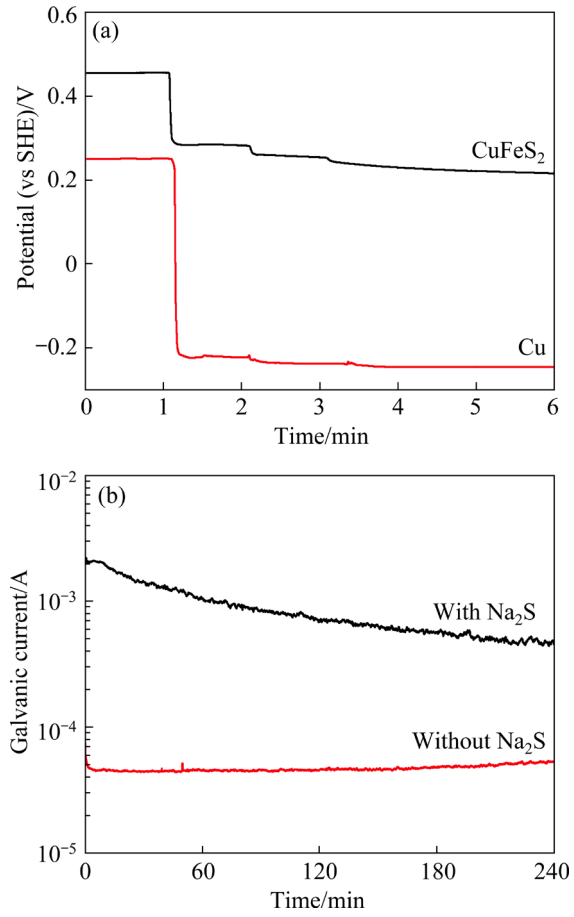

Fig. 9 Electrochemical characterization: (a) OCP under sequential 20 mg Na_2S additions at 1, 2, and 3 min; (b) Galvanic current with or without Na_2S

Under Na_2S-free conditions (Fig. 10(a)), real-time monitoring of sequential phase transitions was achieved through visual observation of surface color evolution: purplish red → blue → gray on $CuFeS_2$ in galvanic contact with copper. Raman spectroscopy analysis (Fig. 10(b)) detected a characteristic vibrational mode at 292 cm^{-1} [35], corresponding to the vibrational mode of pristine $CuFeS_2$. The emergence of metastable phases was marked by a Cu—S stretching band at 474 cm^{-1} (30−60 min), consistent with reference spectra for covellite (CuS) and/or Cu_5FeS_4 [36].

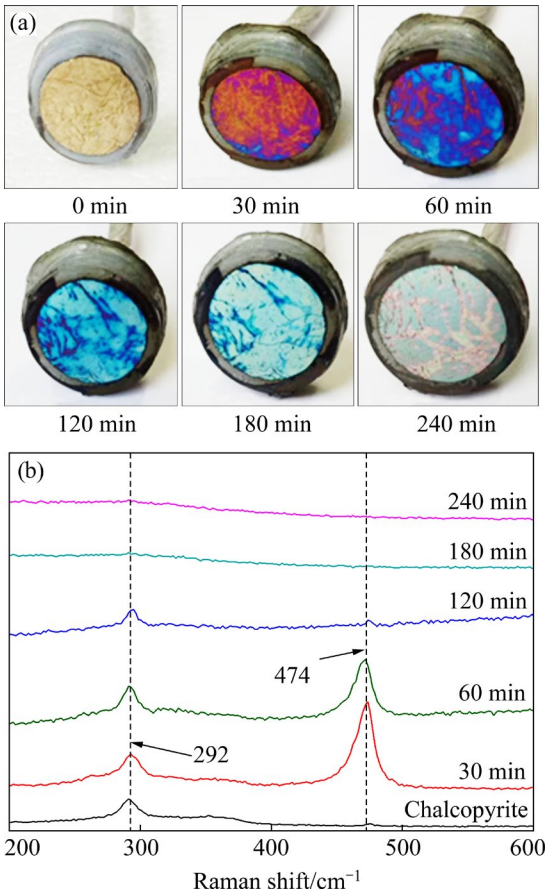

Fig. 10 Surface evolution of $CuFeS_2$ in Cu–$CuFeS_2$ galvanic system (H_2S-free): (a) $CuFeS_2$ electrode discoloration; (b) Raman spectra of surface products

Cross-sectional elemental mapping (Fig. 11(a)) identified a 0.5 μm-thick Fe-depleted layer on $CuFeS_2$ surfaces. EDS analysis of Region A revealed normalized elemental compositions of Cu (52.8%), Fe (9.74%), and S (37.46%), consistent with the stoichiometric ratio of Cu_5FeS_4. However, the rapid release of toxic H_2S after the addition of Na_2S made it difficult to detect the generation process of intermediates. In Na_2S-supplemented system (Fig. 11(b)), granular gray-black precipitates were predominantly observed on $CuFeS_2$ surfaces after 4 h of galvanic testing. EDS quantification confirmed a composition of Cu (63.71%), Fe (1.84%), and S (34.45%), aligning with the chemical signature of Cu_2S.

3.3 Modification of chalcopyrite reductive phase transition process by hydrogen sulfide

The Pourbaix diagram for the Cu−Fe−S−H_2O system (Fig. 12), calculated using FactSage, reveals potential-dependent reduction pathways of $CuFeS_2$

to Cu_5FeS_4, Cu_2S, and metallic Cu. The electrochemical validation experiments at pH 1.5 and 50 °C identify three distinct reduction zones: (1) Cu_5FeS_4 formation (from 0.1 to −0.1 V), (2) Cu_2S formation (from −0.1 to −0.56 V), and (3) metallic Cu generation (<−0.56 V) [37].

The reduction of $CuFeS_2$ by metallic Cu in acidic media proceeds through galvanic corrosion

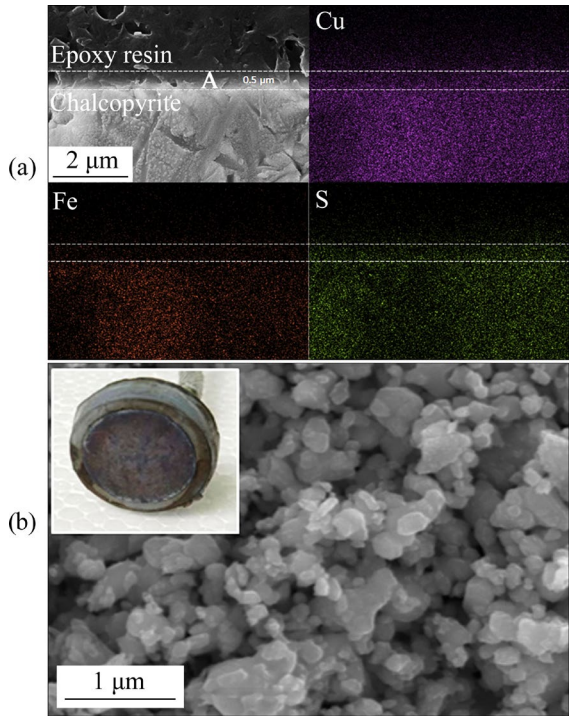

Fig. 11 SEM surface characterization of $CuFeS_2$ sample after galvanic coupling with metallic Cu under distinct environments: (a) H_2S-free system; (b) H_2S-containing system (with 20 mg Na_2S added)

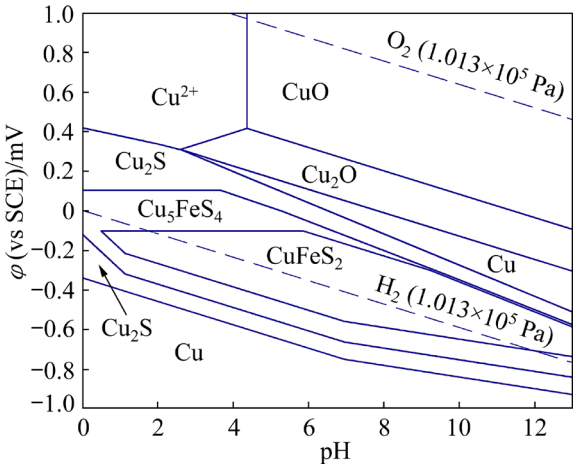

Fig. 12 Pourbaix diagram of Cu−Fe−S−H_2O system (The temperature is 50 °C; the integral quantity is 0.1 mol, x(Fe)/x(Cu+Fe+S)=0.25, x(S)/x(Cu+Fe+S)=0.5)

mechanisms. This process is enhanced by high acidity but inhibited by Cu^{2+}-mediated H_2S removal [38]. Efficient reduction requires two critical conditions: (1) intimate galvanic contact between Cu and $CuFeS_2$ to facilitate electron transfer, and (2) optimal H_2S concentration to modulate redox potentials. Figure 13 details the proposed reaction mechanism. Initial reaction stage involves oxygen-driven H_2S consumption, limiting its availability. The dominant copper oxidation pathway proceeds as follows:

$$Cu{=\!=}Cu^{2+}+2e \quad (4)$$

$CuFeS_2$ primarily reduces to Cu_5FeS_4. This reduction process mainly occurs at the particle surface, and the formation of a tightly coated product layer (Fig. 11(a)) prevents further contact between the inner $CuFeS_2$ and the solution, thereby inhibiting subsequent reduction reactions.

The presence of H_2S allows Cu to be oxidized to Cu_2S at potentials as low as −0.2 V, significantly enhancing its electron-donating capacity:

$$Cu+H_2S{=\!=}Cu_2S+2H^{+}+2e \quad (5)$$

This potential enables concurrent $CuFeS_2$ conversion to Cu_2S conversion and sustains continuous H_2S regeneration, maintaining a low reduction environment. However, H_2S exhibits corrosivity toward Cu, as it can react with Cu to produce H_2 and Cu_2S [39]:

$$Cu+H_2S{=\!=}Cu_2S+H_2{\uparrow} \quad (6)$$

Galvanic coupling drives preferential $CuFeS_2$ reduction at Cu contact interfaces, while unbound Cu reacts with H_2S to produce trace H_2.

When H_2S concentrations exceed critical thresholds, it was demonstrated that introducing 57 g of Na_2S into a 250 mL aqueous solution containing 2 mol/L sulfuric acid yielded substantial yellow precipitates, later identified as elemental sulfur. However, under identical conditions in the presence of hydrochloric acid, H_2S does not undergo oxidation into elemental sulfur by oxygen [40].

Therefore, the redox interaction between H_2S and sulfate ions must be rigorously considered. Thermodynamic calculations and experiments show that H_2S reacts with concentrated sulfuric acid, through two discrete reaction pathways [34]:

$$H_2S+H_2SO_4{=\!=}S+SO_2+H_2O \quad (7)$$

$$2H_2S+SO_2{=\!=}3S+2H_2O \quad (8)$$

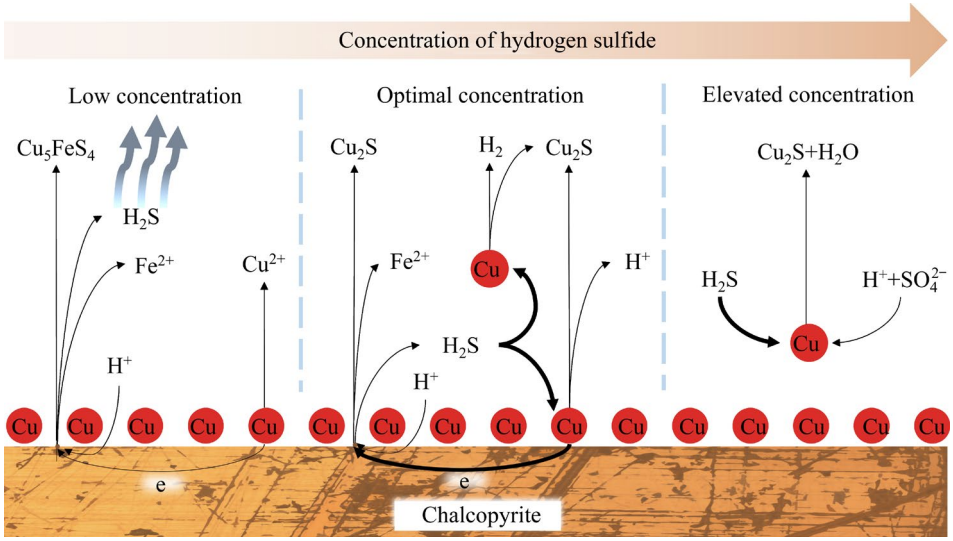

Fig. 13 Schematic diagram of phase transition in Cu reduction of $CuFeS_2$

Experimental results obtained with 1.6 g/L Na_2S addition revealed complete consumption of metallic Cu in leaching residues, accompanied by reduced sulfate ion concentrations and absence of detectable elemental sulfur, indicating modified reaction pathways under Cu-mediated conditions:

$$8Cu+3H_2S+H_2SO_4=4Cu_2S+4H_2O \quad (9)$$

Reaction (9) exhibits strongly negative Gibbs free energy changes (−520.593 kJ/mol at 25 °C and −519.429 kJ/mol at 50 °C), with consistently favorable thermodynamics ($\Delta G<0$) across the studied temperature range. The excessive H_2S concentrations promote non-productive copper consumption, directly impairing $CuFeS_2$ conversion efficiency. The consumption of acid in the reaction may explain the significant reduction in hydrogen gas production. Therefore, it is necessary to conduct in depth exploration of the factors that potentially influence the optimal H_2S concentration. Optimizing this critical parameter will provide essential groundwork for industrial implementation of Cu-mediated $CuFeS_2$ reduction technologies.

4 Conclusions

(1) Without H_2S, the oxidation electrode potential of Cu is 0.251 V, sufficient only for reducing $CuFeS_2$ to Cu_5FeS_4, confined to the particle surface.

(2) The presence of H_2S modifies the oxidation pathway of Cu by lowering its corrosion potential from 0.251 V to −0.223 V, facilitating the complete reduction of $CuFeS_2$ to Cu_2S. The loose morphology of Cu_2S products enhances interfacial reactivity.

(3) Excessive H_2S leads to sulfuric acid reduction, increasing Cu consumption and decreasing $CuFeS_2$ conversion rates. Thus, controlling H_2S levels is crucial for optimizing Cu utilization and ensuring complete $CuFeS_2$ reduction to Cu_2S.

CRediT authorship contribution statement

Xin SUN: Investigation, Methodology, Writing − Original draft, Writing − Review & editing; **Rui LIAO:** Investigation, Writing − Original draft, Writing − Review & editing; **Zu-chao PAN:** Data curation, Conceptualization, Writing − Review & editing; **Yi-sheng ZHANG:** Data curation, Conceptualization, Writing − Review & editing; **Mao-xin HONG:** Formal analysis, Writing – Review & editing; **Yan-sheng ZHANG:** Supervision, Writing – Review & editing; **Jun WANG:** Funding acquisition, Supervision, Writing – Review & editing; **Guan-zhou QIU:** Supervision.

Declaration of competing interest

The authors declare that they have no known competing financial interests or personal relationships that could have appeared to influence the work reported in this paper.

Acknowledgments

This work was financially supported by the National Key Research and Development Program of China (No. 2022YFC2105300).

References

[1] WANG Shi-jie. Copper leaching from chalcopyrite concentrates [J]. JOM, 2005, 57(7): 48−51.

[2] LI Y, KAWASHIMA N, LI J, CHANDRA A P, GERSON A R. A review of the structure, and fundamental mechanisms and kinetics of the leaching of chalcopyrite [J]. Advances in Colloid and Interface Science, 2013, 197: 1−32.

[3] PANDA S, AKCIL A, PRADHAN N, DEVECI H. Current scenario of chalcopyrite bioleaching: A review on the recent advances to its heap-leach technology [J]. Bioresource Technology, 2015, 196: 694−706.

[4] KARTAL M, XIA F, RALPH D, RICKARD W D A, RENARD F, LI W. Enhancing chalcopyrite leaching by tetrachloroethylene-assisted removal of sulfur passivation and the mechanism of jarosite formation [J]. Hydrometallurgy, 2020, 191: 105192.

[5] ZHAO Hong-bo, WANG Jun, GAN Xiao-wen, HU Ming-hao, TAO Lang, QIN Wen-qing, QIU Guan-zhou. Role of pyrite in sulfuric acid leaching of chalcopyrite: An elimination of polysulfide by controlling redox potential [J]. Hydrometallurgy, 2016, 164: 159−165.

[6] NYEMBWE K J, FOSSO-KANKEU E, WAANDERS F, MKANDAWIRE M. pH-dependent leaching mechanism of carbonatitic chalcopyrite in ferric sulfate solution [J]. Transactions of Nonferrous Metals Society of China, 2021, 31(7): 2139−2152.

[7] LIAO Rui, YANG Bao-jun, HUANG Xiao-tao, HONG Mao-xing, YU Shi-chao, LIU Shi-tong, WANG Jun, QIU Guan-zhou. Combined effect of silver ion and pyrite on AMD formation generated by chalcopyrite bio-dissolution [J]. Chemosphere, 2021, 279: 130516.

[8] HONG Mao-xin, WANG Wei, LI Lai-shun, LIU Yang, TONG Li-zhi, QIU Guan-zhou, YANG Bao-jun, WANG Jun. The use of biogenic Fe^{3+} and H_2SO_4 generated from pyrite waste to enhance bornite bioleaching: A potential utilization of acid mine drainage [J]. Minerals Engineering, 2022, 190: 107927.

[9] HONG Mao-xin, LIN Hao, YANG Bao-jun, XIAO Jing, LIAO Rui, YU Shi-chao, ZHAO Chun-xiao, LIU Shi-tong, SUN Xin, WANG Jun, QIU Guan-zhou. Evolution of passivating species on bornite surface during electrochemical dissolution [J]. Transactions of Nonferrous Metals Society of China, 2023, 33(6): 1906−1918.

[10] SANDSTROM A, SHCHUKAREV A, PAUL J. XPS characterization of chalcopyrite chemically and bio-leached at high and low redox potential [J]. Minerals Engineering, 2005, 18(5): 505−515.

[11] CORDOBA E M, MUNOZ J A, BLAZQUEZ M L, GONZALEZ F, BALLESTER A. Leaching of chalcopyrite with ferric ion. Part II: Effect of redox potential [J]. Hydrometallurgy, 2008, 93: 88−96.

[12] HIROYOSHI N, TSUNEKAWA M, OKAMOTO H, NAKAYAMA R, KUROIWA S. Improved chalcopyrite leaching through optimization of redox potential [J]. Canadian Metallurgical Quarterly, 2008, 47(3): 253−258.

[13] ZHAO Hong-bo, WANG Jun, YANG Cong-ren, HU Ming-hao, GAN Xiao-wen, TAO Lang, QIN Wen-qing, QIU Guan-zhou. Effect of redox potential on bioleaching of chalcopyrite by moderately thermophilic bacteria: An emphasis on solution compositions [J]. Hydrometallurgy, 2015, 151: 141−150.

[14] SUN Xin, YUAN Wen-bing, JIN Kai, ZHANG Yan-sheng. Control of the redox potential by microcontroller technology: Researching the leaching of chalcopyrite [J]. Minerals, 2021, 11(4): 382.

[15] DREISINGER D, ABED N. A fundamental study of the reductive leaching of chalcopyrite using metallic iron. Part I: Kinetic analysis [J]. Hydrometallurgy, 2002, 66: 37−57.

[16] HASHEMZADEH M, DIXON D G, LIU W Y. Modelling the kinetics of chalcocite leaching in acidified cupric chloride media under fully controlled pH and potential [J]. Hydrometallurgy, 2019, 189: 105114.

[17] FANG Chao-jun, WANG Jun, QIU Guan-zhou. Advancements on chemical-biological dissolution mechanism and leaching kinetics of chalcocite [J]. Transactions of Nonferrous Metals Society of China, 2024, 34(1): 283−297.

[18] HISKEY J B, WADSWORTH M E. Galvanic conversion of chalcopyrite [J]. Metallurgical Transactions B, 1975, 6: 183−190.

[19] TIAN Zu-yuan, LI Hao-dong, WEI Qian, QIN Wen-qing, YANG Cong-ren. Effects of redox potential on chalcopyrite leaching: An overview [J]. Minerals Engineering, 2021, 172: 107135.

[20] DOYLE F M, LAPIDUS G T. Reductive leaching of chalcopyrite by aluminum [J]. ECS Transactions, 2006, 2(3): 189.

[21] VARDNER J T, GENCER E, EMERSON M, FARINATO R S, NAGARAJ D R, BANTA S, WEST A C. Vanadium(II) sulfate for the reductive leaching of chalcopyrite: Replacing smelting with electrolysis for copper production [J]. ChemElectroChem, 2022, 9(24): e202200920.

[22] VARDNER J T, INABA Y, JUNG H J, FARINATO R S, NAGARAJ D R, BANTA S, WEST A C. The reductive leaching of chalcopyrite by chromium(II) chloride for the rapid and complete extraction of copper [J]. ChemistryOpen, 2023, 12(1): e202200196.

[23] BIEGLER T, CONSTABLE D C. Continuous electrolytic reduction of a chalcopyrite slurry [J]. Journal of Applied Electrochemistry, 1977, 7(2): 175−179.

[24] DONNELLY C A, VARDNER J T, ZHANG Z Y, BANTA S, WEST A C. Impact of anode on product formation during the electrochemical reduction of chalcopyrite [J]. JOM, 2020, 72(11): 3818−3825.

[25] BARRERA-MENDOZA G E, LAPIDUS G T. The effect of chemical additives on the electro-assisted reductive pretreatment of chalcopyrite [J]. Hydrometallurgy, 2015, 158: 35−41.

[26] FUENTES-ACEITUNO J C, LAPIDUS G T, DOYLE F M. A kinetic study of the electro-assisted reduction of chalcopyrite [J]. Hydrometallurgy, 2008, 92: 26−33.

[27] MARTINEZ-GOMEZ V J, FUENTES-ACEITUNO J C, PEREZ-GARIBAY R, LEE J C. A phenomenological study of the electro-assisted reductive leaching of chalcopyrite [J].

Hydrometallurgy, 2016, 164: 54−63.
[28] QIAN Hui-xuan, ZHANG Bo, ZENG Yan-wei, GUO Hong-lei, FENG Zhi-yuan, LEI Bing, ZHANG Ping, MENG Guo-zhe. A new perspective on the mechanism of swift corrosion perforation of copper in solutions containing sulfate-reducing bacteria [J]. Journal of Cleaner Production, 2024, 451: 142117.
[29] PAN Zu-chao, XIONG Jing-jing, CUI Yan-fang, WEI Qian, JIA Wen-hao, ZHANG Zheng-quan, JIAO Fen, QIN Wen-qing. Effect mechanism of carbonaceous materials on the flotation separation of lead-zinc ore [J]. Separation and Purification Technology, 2022, 294: 121101.
[30] LI Hao, WANG Hao, LV Pin, MA Hong-zhi. Bridging thermochemical technology and ecology: Research progress on utilization of FactSage software for environmental applications [J]. Applied Sciences-Basel, 2024, 14(17): 7784.
[31] AMIN M A, KHALED K F. Copper corrosion inhibition in O_2-saturated H_2SO_4 solutions [J]. Corrosion Science, 2010, 52(4): 1194−1204.
[32] KITAI A G, GABLINA I F, BOL'SHIKH A O. Formation of elemental sulfur during the oxidation leaching of chalcocite [J]. Russian Metallurgy, 2022, 2022(5): 463−474.
[33] VELASQUEZ P, LEINEN D, PASCUAL J, RAMOS-BARRADO J R, CORDOVA R, GOMEZ H, SCHREBLER R. XPS, SEM, EDX and EIS study of an electrochemically modified electrode surface of natural chalcocite (Cu_2S) [J]. Journal of Electroanalytical Chemistry, 2001, 510(1/2): 20−28.
[34] WANG Hui, DALLA LANA I G, CHUANG K T. Thermodynamics and stoichiometry of reactions between hydrogen sulfide and concentrated sulfuric acid [J]. Canadian Journal of Chemical Engineering, 2003, 81(1): 80−85.
[35] MAJUSTE D, CIMINELLI V S T, OSSEO-ASARE K, DANTAS M S S, MAGALHAES-PANIAGO R. Electrochemical dissolution of chalcopyrite: Detection of bornite by synchrotron small angle X-ray diffraction and its correlation with the hindered dissolution process [J]. Hydrometallurgy, 2012, 111/112: 114−123.
[36] PARKER G K, WOODS R, HOPE G A. Raman investigation of chalcopyrite oxidation [J]. Colloids and Surfaces A: Physicochemical and Engineering Aspects, 2008, 318(1): 160−168.
[37] LIANG Chang-Li, XIA Jin-Lan, YANG Yi, NIE Zhen-Yuan, ZHAO Xiao-Juan, ZHENG Lei, MA Chen-Yan, ZHAO Yi-Dong. Characterization of the thermo-reduction process of chalcopyrite at 65 °C by cyclic voltammetry and XANES spectroscopy [J]. Hydrometallurgy, 2011, 107: 13−21.
[38] AVRAAMIDES J, MUIR D M, PARKER A J. Cuprous hydrometallurgy. Part VI: Activation of chalcopyrite by reduction with copper and solutions of copper(I) salts [J]. Hydrometallurgy, 1980, 5: 325−336.
[39] TRAN T T M, FIAUD C, SUTTER E M M, VILLANOVA A. The atmospheric corrosion of copper by hydrogen sulfide in underground conditions [J]. Corrosion Science, 2003, 45(12): 2787−2802.
[40] MARTINEZ-GOMEZ V J, FUENTES-ACEITUNO J C, PEREZ-GARIBAY R, LEE J C. A study of the electro-assisted reductive leaching of a chalcopyrite concentrate in HCl solutions. Part I: Kinetic behavior and nature of the chalcopyrite reduction [J]. Hydrometallurgy, 2018, 181: 195−205.

硫化氢对铜还原浸出黄铜矿的影响

孙 欣[1,2]，廖 蕤[1,2]，潘祖超[1]，张伊升[1,2]，洪茂鑫[1,2]，张雁生[1,2]，王 军[1,2]，邱冠周[1,2]

1. 中南大学 资源加工与生物工程学院，长沙 410083；
2. 中南大学 生物湿法冶金教育部重点实验室，长沙 410083

摘 要：通过一系列浸出实验和电化学实验，深入探究了硫化氢 (H_2S) 在铜还原黄铜矿过程中的具体作用。研究结果显示，在无 H_2S 的条件下，金属铜将黄铜矿转化为斑铜矿 (Cu_5FeS_4)。然而，引入 H_2S 后，通过改变铜的氧化路径，可促进辉铜矿 (Cu_2S) 的生成。电化学分析表明，H_2S 的存在使铜的腐蚀电位从 0.251 V 显著降至 −0.223 V (vs SHE)，满足辉铜矿生成所需的临界电位。然而，过量 H_2S 会引发硫酸的还原反应 ($8Cu + H_2SO_4 + 3H_2S = 4Cu_2S + 4H_2O$；$\Delta G$ =−519.429 kJ/mol，50 ℃)，导致铜利用率降低。

关键词：黄铜矿还原；铜；硫化氢；辉铜矿

(Edited by Bing YANG)